J MATER SCI **41** (2006) 2621–2625

Dislocation structures of low-angle boundaries in Nb-doped $SrTiO_3$ bicrystals

S. -Y. CHOI
Institute of Engineering Innovation, University of Tokyo, 2-11-18 Yayoi Bunkyo-ku, Tokyo, 113-8656, Japan; Department of Materials Science and Engineering, Korea Advanced Institute of Science and Technology, Daejeon, 305-701, Korea

J. P. BUBAN
Institute of Engineering Innovation, University of Tokyo, 2-11-18 Yayoi Bunkyo-ku, Tokyo, 113-8656, Japan

M. NISHI, H. KAGEYAMA
Department of Advanced Materials Science, University of Tokyo, 7-3-1 Hongo Bunkyo-ku, Tokyo, 113-8656, Japan

N. SHIBATA
Institute of Engineering Innovation, University of Tokyo, 2-11-18 Yayoi Bunkyo-ku, Tokyo, 113-8656, Japan

T. YAMAMOTO
Department of Advanced Materials Science, University of Tokyo, 7-3-1 Hongo Bunkyo-ku, Tokyo, 113-8656, Japan

S. -J. L. KANG
Department of Materials Science and Engineering, Korea Advanced Institute of Science and Technology, Daejeon, 305-701, Korea

Y. IKUHARA
Institute of Engineering Innovation, University of Tokyo, 2-11-18 Yayoi Bunkyo-ku, Tokyo, 113-8656, Japan

Published online: 17 April 2006

Dislocation core structures in low-angle boundaries of Nb-doped $SrTiO_3$ bicrystals were investigated by high-resolution electron microscopy. Bicrystals with tilt angles of 2°, 4°, 6° and 8° with respect to the [001] zone axis were prepared by joining two single crystals at 1873 K. All of the boundaries consisted of a regular array of dislocations whose spacing gradually decreased with an increase in tilt angle. Except for the 2° tilt-angle boundary, the dislocation cores exhibited a dissociation from **a**[010] into two partials of **a**/2[010] on (100). Furthermore, two kinds of dislocation core structures were observed; Sr–Sr atomic columns and Ti–O atomic columns inside the cores. In addition, it was found that the positioning of adjacent cores along the boundary tended to change from a linear form to a zig-zagg shape as the tilt angle was increased from 4° to 8°. In the case of the linear array, dislocation core structures including Sr–Sr columns or Ti–O columns alternately appear. In contrast, only one core structure was observed in the zig-zagged array. On the other hand, the dislocation cores in the 2°-tilt-angle boundary had another type of dissociation with **a**/2[110] or **a**/2[111] partials, which included the twist component at a tilt axis of [001].

0022-2461
DOI: 10.1007/s10853-006-7824-9

1. Introduction

Some perovskite structured ceramics such as $SrTiO_3$ and $BaTiO_3$ have been used in various electronic components, for example varistors [1], grain-boundary layer capacitor (GBLC) [2], positive temperature coefficient (PTC) resistor [3, 4] and so on. Such electrical properties primarily depend on grain-boundary characteristics which are strongly correlated with the potential barrier as well as the resultant microstructure [5–7]. So far, many researchers have reported that the electrical properties across single grain boundaries exhibit a dependency of grain-boundary coherency [8–10]. According to their reports, the remarkable electrical properties appear at random type boundaries, while, in the highly coherent boundaries, the electrical properties are similar to those in single crystals. Recently, non-linearity in current-voltage behaviors in Nb-doped $SrTiO_3$ was found to show the tilt angle dependency even in the highly coherent boundary, i.e., the low-angle boundaries, which consist of a regular array of grain-boundary dislocations [11]. These results imply that the arrangement of dislocations and their core atomic structures are closely related to the formation of potential barriers. As for the grain-boundary structure in low-angle boundaries in $SrTiO_3$, it was reported that the dislocation core in the low-angle boundary has a unique structure [12, 13]. Zhang *et al*. [12] have revealed that the grain-boundary dislocations exhibit a dissociation $\mathbf{a}[010] \rightarrow \mathbf{a}/2[010] + \mathbf{a}/2[010]$ in a [001] tilt boundary with a misfit angle of 5.4°. By this dissociation, two different types of dislocation cores consisting of Sr–Sr or Ti–O atomic columns alternately appear along a grain boundary. In order to understand the tilt-angle dependency of electrical properties in low-angle boundary of $SrTiO_3$, it is necessary to know the variation of such dislocation structures caused by tilt angles.

In this study, an analysis on the dislocation core structures was intensively performed using Nb-doped $SrTiO_3$ bicrystals. To identify the dislocation core structure, various types of low-angle boundaries, with 2°, 4°, 6° and 8° tilt angles, were fabricated by a diffusional bonding method. The change in the arrangement of the dislocation cores and their core structures were investigated as the tilt angle increased.

2. Experimental procedure

The [001] symmetric tilt boundaries with tilt angles of 2°, 4°, 6° and 8° were fabricated by joining two single crystals as shown in Fig. 1. For joining, commercial $SrTiO_3$ single crystals doped with 0.2 at% Nb were used. The crystal size was $10 \times 10 \times 3$ mm^3. The broad 10×10 mm^2 face, inclined at half of the desired tilt angle from (010), was prepared for a contacting plane. The contacting planes of the single crystals were ground and polished to a mirror finish with 0.25 μm diamond slurry. Then, two single crystals were stacked to adjust the edges of the respective single crystals, and the stacked pair was heated at 1873 K for 10 h in air. Heating and cooling rates were 200 K/h in this joining process. After joining, some plates with a size of $10 \times 10 \times 1$ mm^3 were cut from the bicrystals for TEM sample preparation as schematically shown in Fig. 1. The thin foils for HRTEM observation were prepared using a conventional method including mechanical thinning to $\sim$20 μm and ion beam milling to electron transparency at an acceleration voltage of 2–4 kV using an Ar ion beam. The grain boundary atomic structures were investigated using high-resolution transmission electron microscopes (JEOL JEM-4010, JEOL Co., Ltd. and EM-002BF, TOPCON) operated at 400 kV and 200 kV, respectively.

3. Results and discussion

Fig. 2 shows a series of HRTEM images from the low-angle tilt boundaries prepared in this study. All of the boundaries are perfectly joined in the preparation condition, and no intergranular phase exists even on an atomic scale. A tilt misorientation of the adjacent crystals causes to the formation of isolated dislocations in a regular array as indicated by the arrows in Fig. 2. The spacing of the dislocations decreases with an increase in the tilt angles, i.e., 11.2, 5.3, 3.7 and 2.7 nm, respectively. On the other hand, the contrast of dislocation cores in the 2°-tilt-angle boundary is significantly different to the others. In addition, there appear to be two different types of core structures in the case of the 2°-tilt-angle boundary, in contrast to the 4°, 6° and 8°-tilt-angle boundaries that exhibit similar contrast at the dislocation cores. The contrast of dislocation cores indicated by the white arrows seems to be totally different from that of dislocation cores indicated by black arrows, as shown in Fig. 2a. Such a difference in the contrast implies that the Burgers vectors in the 2°-tilt-angle boundary may be totally different from those in the other boundaries. Detailed discussion will be given at the end of this section.

Fig. 3 shows an enlarged HRTEM image of the 4°-tilt-angle boundary. In this figure, the atomic columns and Burgers circuits are shown schematically. From a [001] view of the $SrTiO_3$ lattice, there exist three kinds of atomic columns: Sr–Sr, Ti–O and O–O. The white contrasts in the image are coincident to the positions of O–O columns as shown schematically with a unit cell. The positions of the two other columns including cations, i.e., Sr–Sr and Ti–O columns, are shown with the white or black dots and hereby the two kinds of dislocation cores are defined by the double circled dots. In this image, one atomic plane of A–A' commonly goes through the two dislocation cores, which means the two dislocation cores are positioned on the same atomic plane. The atomic columns between the two cores have a different type from those in the neighboring areas along the common plane of A–A and thus the cores have two kinds of structures; one is a Sr–Sr

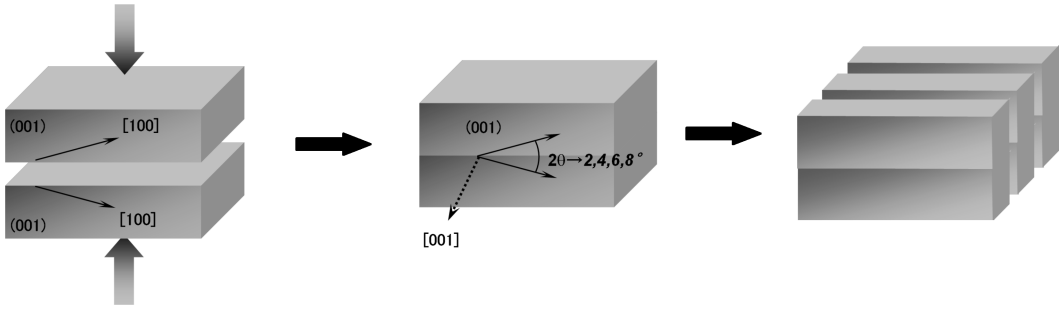

Figure 1 Schematics of the sample preparation procedure and an orientation relationship of two single crystals.

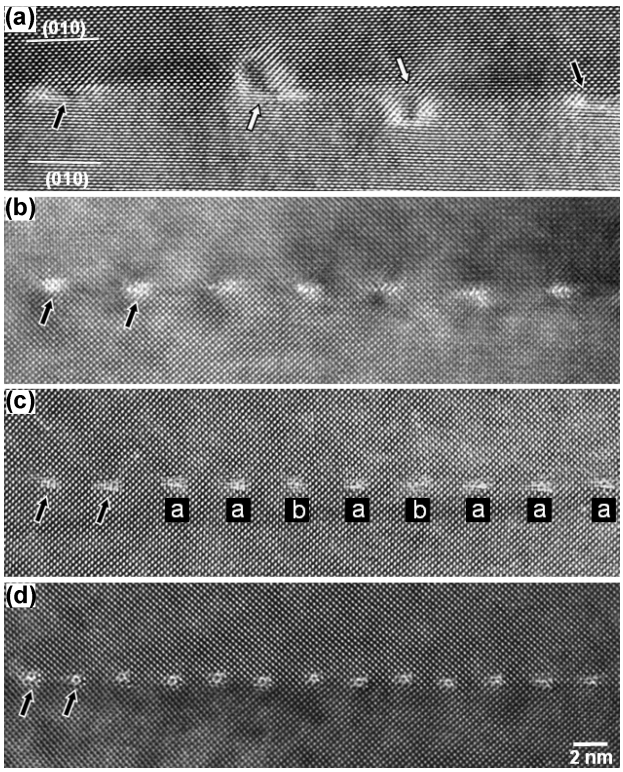

Figure 2 A series of HRTEM images from the bicrystals with tilt angles of (a) 2°, (b) 4°, (c) 6° and (d) 8°.

column type and the other a Ti–O one as indicated with double circled dots. This change in the array of the cation columns gives no change in a stacking sequence normal to the common plane. As recognized in the Burgers circuits, the dislocations seem to have **a**[010]-type Burgers circuits, where **a** is the lattice parameter of the $SrTiO_3$ lattice, 0.3905 nm. The Burgers vector of **a**[010], however, dissociates into two **a**/2[010] because an atomic plane exists inside the apparent dislocation core. This unique arrangement in dislocation cores is very similar to the previous result of non-doped $SrTiO_3$ bicrystal with 5.4° tilt angle reported by Zhang *et al*. [12] which shows an energetically stable dislocation core structure in the low-angle boundary.

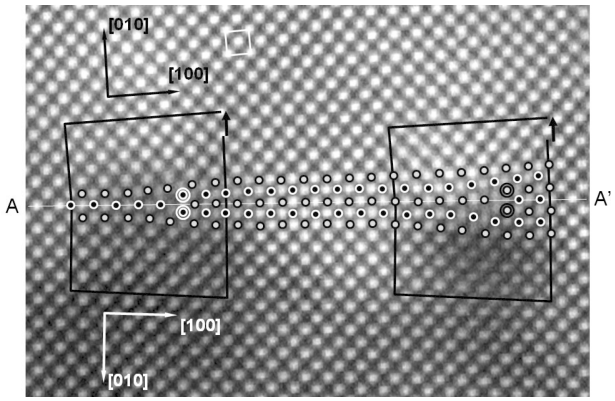

Figure 3 Enlarged HRTEM image of the 4°-tilt-angle boundary showing the dislocation cores in a line. The white square indicates the unit cell on (001) plane.

In comparison with the dislocation cores of the 4°-tilt-angle boundary, as the tilt angle is increased, the position of the dislocation cores apparently form a zig-zag line along the grain-boundary plane of ∼(100) in the 6°-tilt-angle boundary. The change in the array of dislocation cores keeps pace with two types of contrasts of dislocation cores, as indicated by **a** and **b** in Fig. 2c. For example, three dislocation cores in regular sequence of **a a a** are in a zig-zagged array and another three, **a b a**, are on the same atomic plane (in-line) array. Fig. 4 shows HRTEM images of (a) the in-line dislocations and (b) the zig-zag dislocations taken from the 6°-tilt-angle boundary. In the case of the in-line type as shown in Fig. 4a, the dislocation core structure is similar to that recognized in the 4° boundary as shown in Fig. 3. The sequence of atomic columns also changes alternately at the portion of the dislocation cores and thus *A* and *B* have a different core structures, i.e., different types of cation columns. On the other hand, Fig. 4b shows the shifted type of dislocation cores. It can be also seen that three dislocation cores seem to have the similar contrast. Therefore, in the case of the shifted array, the atomic column at the core has a similar type.

This unique positioning can be also seen more clearly in the 8°-tilt-angle boundary, as shown in Fig. 5a. As shown in Figs 2d and 5a most of the dislocation cores have

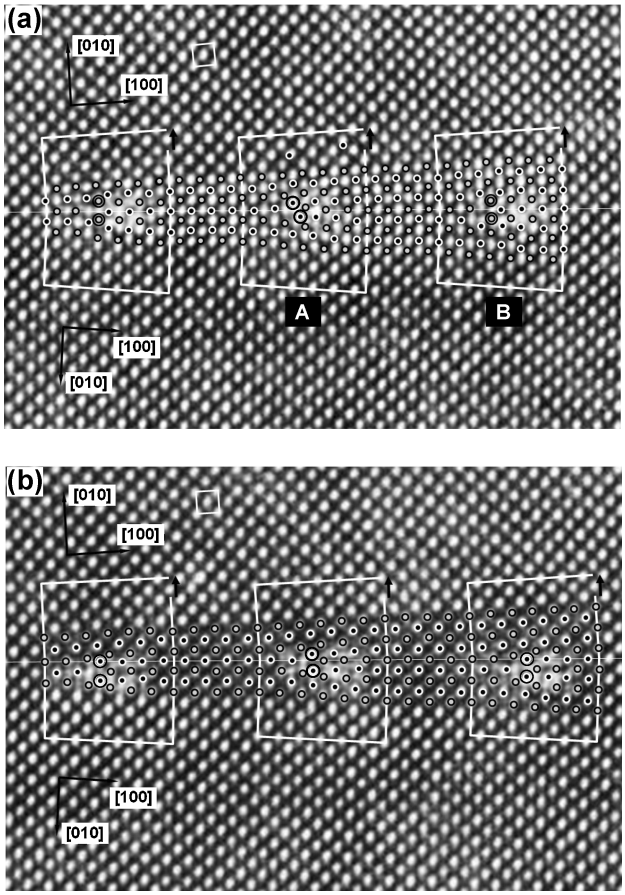

Figure 4 Enlarged HRTEM images of the 6°-tilt-angle boundary showing the dislocation cores (a) in a line and (b) in a zig-zag. The white square indicates the unit cell on the (001) plane.

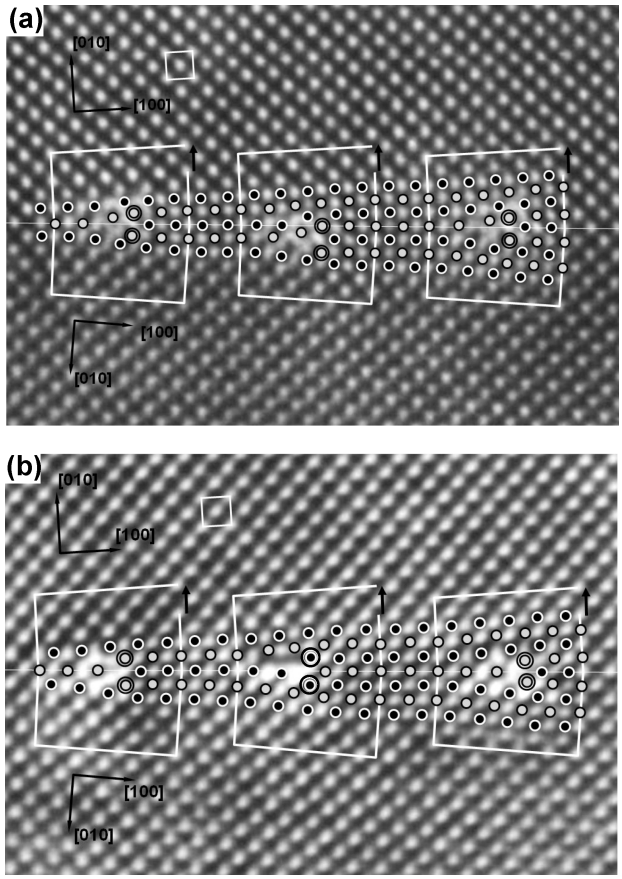

Figure 5 Enlarged HRTEM images of the 8°-tilt-angle boundary showing the dislocation cores (a) in a zig-zag and (b) in a line. The white square indicates the unit cell on the (001) plane.

similar contrast as predicted by a positioning feature of the zig-zagged array. Besides the shifted dislocation cores in the 8° boundary, the in-line dislocation cores can be also observed, as shown in Fig. 5b. However, areas of such in-line dislocation cores were observed in fewer than 20% of the HRTEM images taken from the 8°-tilt-angle boundary. Therefore, these experimental results from the 4°, 6° and 8°-tilt-angle boundaries imply that, as the tilt angle is increased, the energetically more stable core structure, either of Sr–Sr or Ti–O columns, predominates, which must be producing the zig-zag dislocation cores.

Differing from the 4°, 6° and 8°-tilt-angle boundaries, the 2°-tilt-angle boundary consists of two types of dislocation, as distinguished by the different contrasts, as shown in Fig. 2a. The dislocation contrast indicated by white arrows seem to be totally different from that indicated by black arrows in Fig. 2a. In this case, the respective dislocations dissociate into two partials with a twist component. Fig. 6 shows enlarged images taken from the dislocations as indicated by (a) the black and (b) the white arrows in Fig. 2a, respectively. The Burgers circuits drawn around the two partial dislocations show that the total Burgers vector projected on (001) is **a**[010]. Both of the two dislocations in Figs 6a and b, however, dissociate into the dislocations whose component on (001) is **a**/2<110>. Considering the perovskite structure, in this case, two candidate partial dislocations having an edge component of **a**/2<110> are **a**/2<110> and **a**/2<111>. On the other hand, the spacing between the two partials is larger in the dislocation in Fig. 6a. Considering the magnitude of the Burgers vector of the partial dislocation, it can be considered that **a**/2[111] may be energetically favorable in the case of the dislocation in Fig, 6a.

On the assumption that a pure tilt boundary without a twist component is made up of pure edge dislocations, the spacing, d_{th} between dislocations can be expressed by Frank's formula [14]:

$$d_{th} = \frac{|b|}{2\sin(\theta/2)}$$

where$|b|$ is the modulus of the Burgers vector, andθ is a tilt angle. Table I shows the spacing estimated from Frank's formula using edge component of **a**[010]. In the table, the results obtained from the other boundaries are also shown. The values deduced from Frank's formula

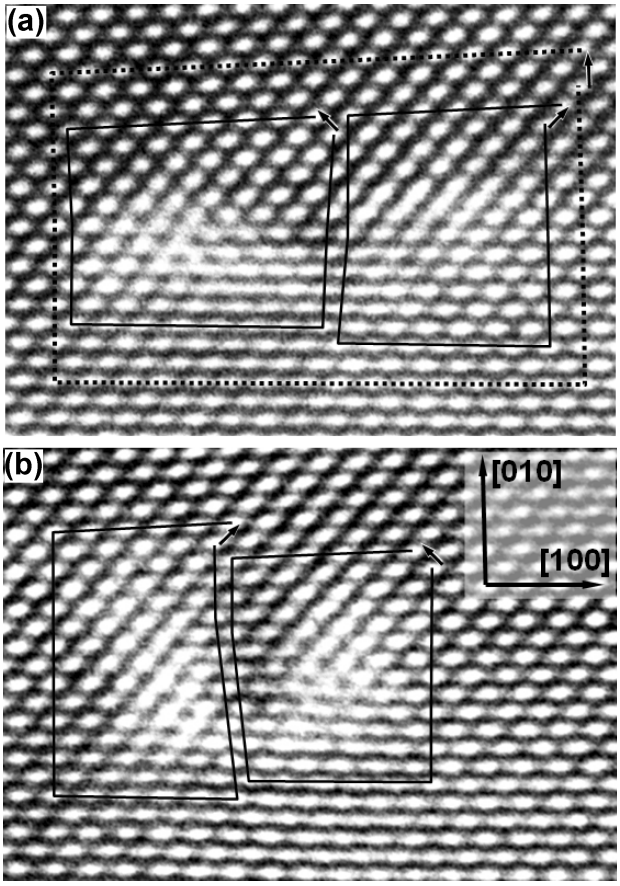

Figure 6 Enlarged HRTEM images of the 2°-tilt-angle boundary.

are in good agreement with the experimental ones. This implies that, even though the all dislocation cores are dissociated into two partials in this study, such dissociation may be induced by the pure edge dislocation. Therefore, the Burgers vector in the 2°-tilt-angle boundary can be also considered to have totally edge type of **a**/2[010].

4. Conclusion

Four kinds of the low-angle boundaries having 2°, 4°, 6° and 8° tilt angles were successfully fabricated. In all the boundaries, isolated dislocations were observed. By increasing the tilt angle, the spacing between dislocations was gradually decreased. In the 4°, 6° and 8°-tilt-angle boundaries, the dislocation core consisted of two partial dislocations with **a**/2[010]. In the 4°-tilt-angle boundary, most of dislocation cores were in a line and Sr–O and Ti–O core structures appeared alternately. In the 6° and 8°-tilt boundaries, there were two arrangements of the dislocation cores; one was in a line and the other one was zig-zagged. The percentage of the zig-zagged dislocation cores in the 8°-tilt-angle boundary was greater than in the 6°-tilt-angle boundary. In the case of zig-zagged type, only dislocation cores containing either of Sr–Sr columns or Ti–O columns were linear. On the other hand, in the 2°-tilt-angle boundary, dissociation of the dislocation with **a**/2[110] or **a**/2[111] was observed. However, the spacing between the dislocation cores in all boundaries was in considerable agreement with values deduced by Frank's formula using **a**[010]. Therefore, it can be concluded that the dissociation with **a**/2[110] or **a**/2[111] in the 2°-tilt-angle boundary might have originated from the dissociation with **a**/2[010] like the other boundaries.

References

1. M. FUJIMOTO, Y.-M. CHIANG, A. ROSHKO and W. D. KINGERY, *J. Am. Ceram. Soc.* **68** (1985) C300.
2. R. WERNICKE, "Formation of second-phase layers in $SrTiO_3$ boundary layer capacitors, in Grain Boundary Phenomena in Electronic Ceramics, Advances in Ceramics vol. 1, Edited by L. M. Levinson (American Ceramic Society, Columbus, OH, 1981).
3. W. HEYWANG, *J. Am. Ceram. Soc.* **47** (1964) 484.
4. G. H. JONKER, *Solid State Electron.* **7** (1964) 895.
5. D. HENNINGS, R. JANSSEN and P. REYNEN, *J. Am. Ceram. Soc.* **70** (1987) 23.
6. Y.-I. JUNG, S.-Y. CHOI and S.-J. L. KANG, *ibid.* **86** (2003) 2228.
7. S.-Y. CHOI and S.-J. L. KANG, *Acta Mater.* **52** (2004) 2973.
8. H. NEMOTO and I. ODA, *J. Am. Ceram. Soc.* **63** (7/8) (1980) 398.
9. K. HAYASHI, T. YAMAMOTO and T. SAKUMA, *ibid.* **79** (1996) 1669.
10. M. KUWABARA, K. MORIMO and T. MATSUNAGA, *ibid.* **79** (1996) 997.
11. T. YAMAMOTO, F. OBA, Y. IKUHARA and T. SAKUMA, *Mater. Trans.* **43** (2002) 1537.
12. Z. ZHANG, W. SIGLE and M. RÜHLE, *Phys. Rev. B* **66** (2002) 094108.
13. Z. ZHANG, W. SIGLE, W. KURTZ and M. RÜHLE, *Phys. Rev. B* **66** (2002) 214112.
14. A. P. SUTTON and R. W. BALLUFFI, (eds.) "Interfaces in Crystalline Materials," (Clarendon Press, Oxford, 1995).